

Letter

Iliia Sokolovskii and Gerrit Groenhof*

Photochemical Initiation of Polariton Propagation

Abstract: Placing a material inside an optical cavity can enhance transport of excitation energy by hybridizing excitons with confined light modes into polaritons, which have a dispersion that provides these light-matter quasi-particles with low effective masses and very high group velocities. While in experiments polariton propagation is typically initiated with laser pulses, tuned to be resonant either with the polaritonic branches that are delocalized over many molecules, or with an uncoupled higher-energy electronic excited state that is localized on a single molecule, practical implementations of polariton-mediated exciton transport into devices would require operation under low-intensity incoherent light conditions. Here, we propose to initiate polaritonic exciton transport with a photo-acid, which upon absorption of a photon in a spectral range not strongly reflected by the cavity mirrors, undergoes ultra-fast excited-state proton transfer into a red-shifted excited-state photo-product that can couple collectively with a large number of suitable dye molecules to the modes of the cavity. By means of atomistic molecular dynamics simulations we demonstrate that cascading energy from a photo-excited donor into the strongly coupled acceptor-cavity states can indeed induce long-range polariton-mediated exciton transport.

Keywords: Strong light-matter coupling; exciton-polariton; Fabry-Pérot cavity; Quantum Chemistry; Quantum Optics; Molecular Dynamics; exciton transport

1 Introduction

Organic opto-electronic materials offer many advantages over their silicon counterparts, such as lower

production cost, smaller weight, higher flexibility and easier disposability, but are hampered by low exciton mobility [1]. Enhancing that mobility therefore has become a major optimization target and several solutions have been proposed, which include increasing the lifetime via triplet formation [2, 3], ordering molecules to increase exciton delocalization [4–7], or coupling the excitons to the confined light modes of an optical resonator [8–16]. Because the latter solution does not require chemical modifications of the molecules, which may compromise other properties, utilizing strong light-matter coupling could be a promising route towards improving the performance of organic opto-electronic devices.

Because the confinement of light into smaller volumes by an optical resonator increases the interaction with molecular transitions [17], the enhanced exciton mobility in the strong coupling regime has been attributed to hybridization of excitons and confined light modes into polaritons [18–23], which can form when the interaction strength exceeds the decay rates of both excitons and cavity modes [24, 25]. The hybrid states with contributions from cavity modes are bright and can hence be accessed optically [26, 27]. Because the cavity mode energy depends on the in-plane momentum, or wave-vector, k_z , these states have dispersion and form the upper and lower polaritonic branches, as shown in Figure 1f. These branches are separated by the Rabi splitting, which is defined as the energy gap at the wave-vector for which the energy of the exciton and cavity dispersion are resonant. Most of the hybrid states, however, have negligible contribution from the cavity modes, and are hence dark [28]. These dark states therefore also lack dispersion and form a quasi-degenerate manifold instead that is situated in between the two bright polaritonic branches.

Owing to their dispersion, the bright polaritonic states support ballistic motion of population at their group velocity (*i.e.*, $v_g = \partial\omega(k_z)/\partial k_z$, with $\hbar\omega(k_z)$ the energy of a polariton with in-plane momentum k_z , Figure 1f) [15, 18, 19, 22, 23, 29, 30]. However, while in inorganic micro-cavities, such ballistic propagation was

Iliia Sokolovskii, Nanoscience Center and Department of Chemistry, University of Jyväskylä, P.O. Box 35, 40014 Jyväskylä, Finland, ilia.i.sokolovskii@jyu.fi; 0000-0003-3367-0660

*Corresponding author: Gerrit Groenhof, Nanoscience Center and Department of Chemistry, University of Jyväskylä, P.O. Box 35, 40014 Jyväskylä, Finland, gerrit.x.groenhof@jyu.fi; 0000-0001-8148-5334

indeed observed [31, 32], transport in organic microcavities is a diffusion process because of rapid dephasing in disordered organic materials [19]. Results from molecular dynamics (MD) simulations suggest that such dephasing is due to reversible exchange of population between the stationary dark states and propagating polaritonic states [13, 33, 34]. Although polariton-mediated exciton transport is not ballistic in organic systems, polaritonic diffusion can still dramatically outperform the intrinsic exciton diffusivity of the material [9, 16]. However, despite several experimental realizations [8, 9, 13, 14, 16], and an emerging theoretical understanding of polariton propagation in organic microcavities [18–23, 29, 30, 35], strong light-matter coupling has so far not been leveraged systematically for practical applications.

One of the obstacles on the path to polaritonic devices for enhanced exciton transfer is that polariton propagation requires laser excitation of either wavepackets of polaritonic states [11, 14], or higher-energy electronic states of the molecules [8–10, 16]. Yet, for practical applications, such as light-harvesting, it will be essential that transport can also be initiated with low-intensity incoherent light sources. To address this specific challenge for a Fabry-Pérot optical resonator, we propose to initiate polariton propagation in a strongly coupled molecule-cavity system with a suitable donor that, upon excitation at wavelengths for which the cavity mirrors are more transparent [36], undergoes a rapid photo-chemical reaction into an excited-state photo-product with an emission maximum that is resonant with both the cavity and acceptor dye molecules. As illustrated in Figures 1 and 2, such system could potentially be realized if we combine 10-hydroxybenzo[h]quinoline (HBQ) that upon excitation at 375 nm or 360 nm undergoes ultra-fast excited-state intra-molecular proton transfer (ESIPT) on a femtosecond timescale into a photo-product with a broad emission centered at 620 nm [37, 38], with Methylene Blue (MeB) in an optical micro-cavity made of silver mirrors and resonant with the broad absorption peaks of MeB at 668 nm or 609 nm (Figure S3, in the Supplementary Material). Here, we demonstrate the feasibility of this concept, which is somewhat similar to radiative pumping of the LP of a strongly-coupled dye with the emission of a weakly coupled second dye [39], or to the photo-transformation of an uncoupled reactant into a coupled photo-product [36, 40], by means of multi-scale molecular dynamics simulations [41, 42].

2 Materials and Methods

In the simulations, the details of which can be found in the Supplementary Material (SM), a single HBQ molecule solvated in cyclohexane, was combined with 1023 hydrated MeB molecules. While the number of molecules in real cavities is estimated to be much higher (*i.e.*, $10^5 - 10^8$ [28, 43, 44]), we could show in previous work that for modeling polariton propagation, including 1024 molecules in the simulation provides a reasonable compromise [33]. The electronic ground (S_0) and excited (S_1) states of HBQ were modeled with Density Functional Theory (DFT) [45] and time-dependent density functional theory (TDDFT) [46] within the Tamm-Dancoff approximation (TDA) [47], respectively, using the CAM-B3LYP functional [48, 49] in combination with the 3-21G basis set [50]. The cyclohexane solvent molecules were modelled with the GROMOS 2016H66 force field [51]. At this level of theory the vertical excitation energy of HBQ is $h\nu^{\text{HBQ}} = 4.06$ eV (305 nm), while the energy gap to the ground state is 2.58 eV (480 nm) in the S_1 minimum. Despite the overestimation of the S_1 - S_0 energy gap, our model provides potential energy surfaces (Figure 1d) that are in qualitative agreement with the more accurate description at the TPSSh/cc-pVDZ level of theory for this system (Figure S4 in SM) [52, 53]. The S_0 and S_1 electronic states of MeB were modelled with DFT and TDDFT based on the Casida equations [54], respectively, using the B97 functional [55] and the 3-21G basis set. The water molecules were described with the TIP3P model [56]. Although at this level of theory the vertical excitation energy of MeB is $h\nu^{\text{MeB}} = 2.5$ eV, and thus significantly overestimated with respect to experiment, there is a fortuitous overlap with the emission of HBQ that we exploit in this work (Figure 1e). Thus, while MeB may not be the optimal choice for a practical realization, this dye should be suitable for demonstrating the feasibility of inducing polariton-mediated exciton transfer with a photo-chemical reaction in our simulations.

We modelled the optical resonator as a one-dimensional Fabry-Pérot cavity [57] with 239 discrete modes (Figure 1f) and a cavity vacuum field strength of 0.21 MVcm $^{-1}$ (0.00004 au). The fundamental mode at $k_z = 0$ was red-detuned by 323 meV with respect to the excitation maximum of MeB (2.5 eV at the TD-B97/3-21G level of theory). To maximize light-matter coupling, the transition dipole moments of the molecules were aligned with the vacuum field of the

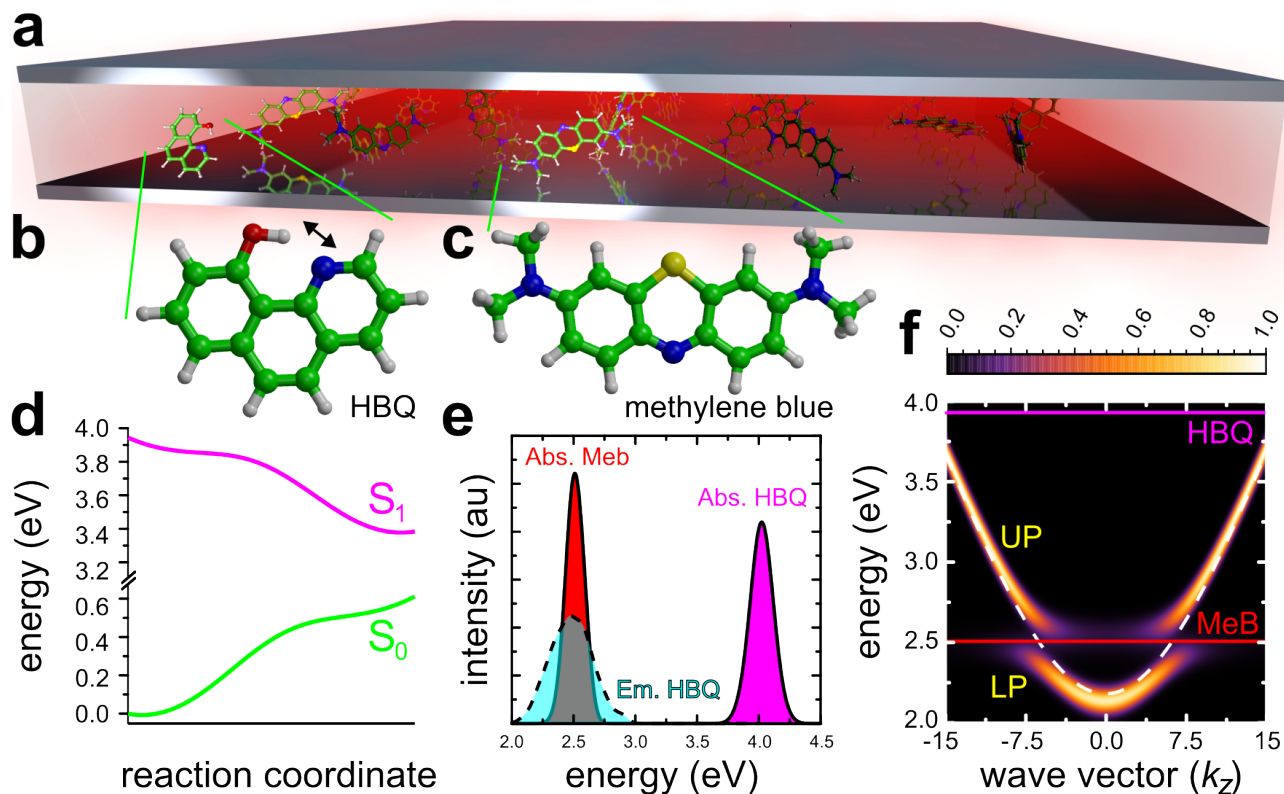


Fig. 1: Illustration of a Fabry-Pérot microcavity (panel a, not to scale) containing a 10-hydroxybenzo[h]quinoline donor molecule (HBQ, panel b) and 1023 Methylene Blue acceptor molecules (MeB, panel c). The first singlet excited states (S_1) of the MeB molecules are coupled to the 239 modes of the cavity. Upon absorbing a photon at a frequency where the mirrors have become more transparent (~ 4.0 eV at the TDA-CAMB3LYP/3-21G level of theory, Figure S3 in SM), HBQ undergoes ultra-fast intra-molecular proton transfer on the S_1 excited-state potential energy surface (panel d) into an excited-state photo-product that is resonant with both the absorption maximum of MeB and the cavity. Panel e shows the QM/MM absorption (magenta) and emission (cyan) spectra of HBQ and the absorption spectrum of MeB (red). The normalised angle-resolved absorption spectrum of the molecule-cavity system (panel f) shows the Rabi splitting of 282 meV between the lower polariton (LP) and upper polariton (UP) branches. The cavity dispersion is plotted as a white dashed line, while the excitation maxima of the MeB molecules (~ 2.5 eV at the TD-B97/3-21G level of theory) and HBQ are plotted as straight red and magenta lines, respectively.

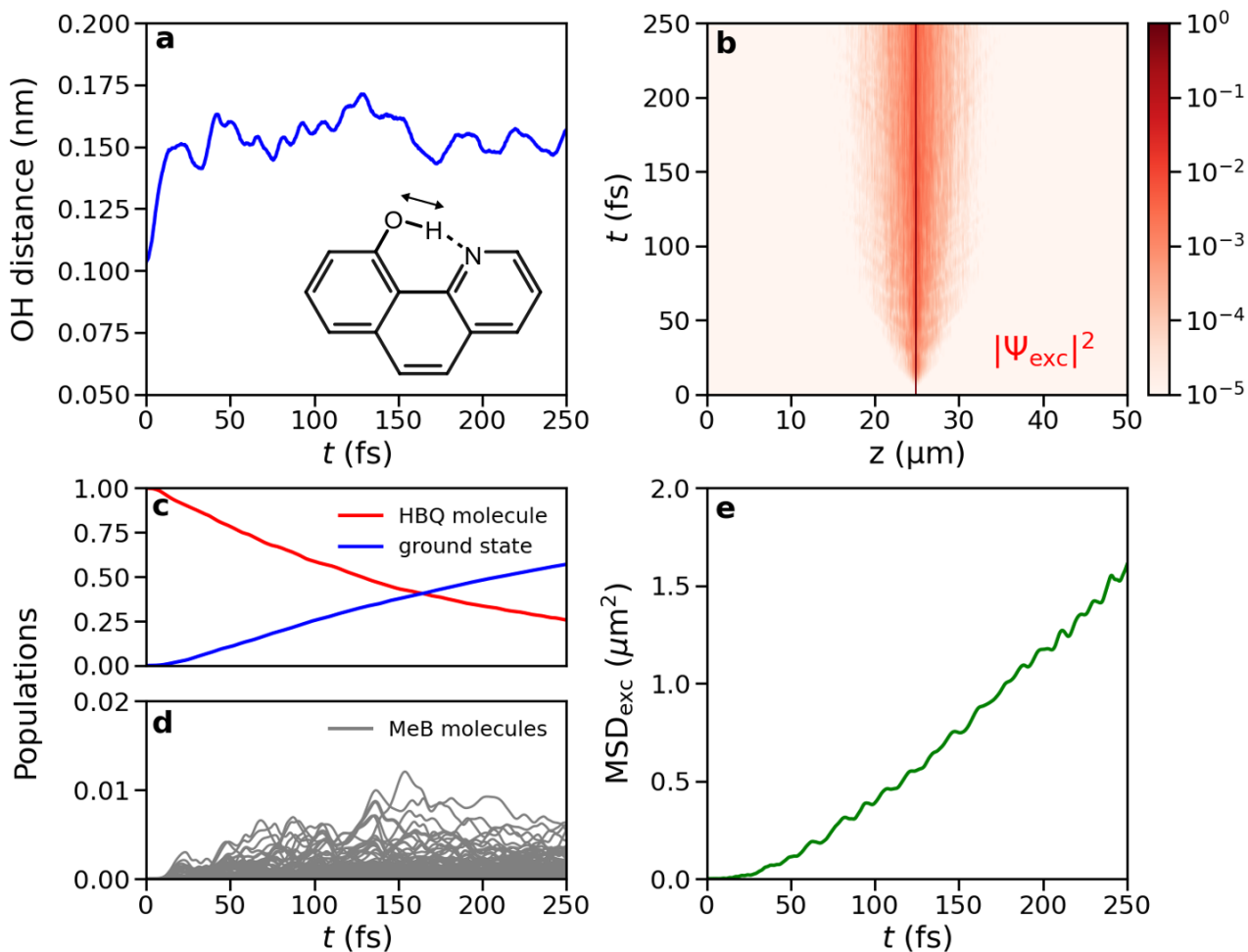


Fig. 3: Panel a shows the distance between the oxygen and proton, which we use as the reaction coordinate for the excited-state proton transfer reaction (inset and see also Figure 1c) as a function of time after instantaneous excitation into the highest energy eigenstate of the molecule-cavity system, which is dominated by the S_1 state of HBQ (*i.e.*, $|\beta_{\text{HBQ}}|^2 \approx 0.99$, panel c). Panel b depicts the probability density of the excitonic part of the wave function $|\Psi_{\text{exc}}|^2$ as a function of the z -coordinate (horizontal axis) and time (vertical axis). Panels c and d show the contribution of the HBQ molecule (red) and the Methylene Blue molecules (grey) to the total wave function, as well as the population of the ground state (blue). Panel e shows the Mean Squared Displacement (*i.e.*, $\text{MSD}_{\text{exc}} = \langle z(t) - z(0) \rangle^2$) of the excitonic wavepacket.

with group velocity, on the other hand, the propagation appears as a diffusion process, indicated by the linear increase of the MSD (Figure 3b) [33]. The observation of diffusion rather than ballistic motion, is in line with experiments on organic micro-cavities [9].

The initial structures for our simulations were sampled from equilibrium QM/MM trajectories at 300 K (SM) and therefore can capture the heterogeneity as indicated by the absorption line-widths of the molecules in Figure 1e. Because of such structural disorder, the ESIPT reaction rates span a distribution. To confirm that the proton transfer in HBQ initiates the polariton-mediated exciton transport process, we show in Figure S5 (SM) that for a system in which the ESIPT is delayed, also the transport starts at a later point in time, and that this time point coincides with the formation of the HBQ photo-product.

4 Conclusion

To summarize, the results of our MD simulations suggest that long-range polariton-mediated exciton transport can be induced with an excited-state proton transfer reaction. While the excitation scheme proposed here resembles the off-resonant laser excitation conditions employed in previous experiments of polariton transport [8, 9, 13, 16], the absorption cross-section of HBQ should be high enough to initiate the propagation with incoherent light, in particular for a cavity with a thin silver top mirror, which is more than 50% transparent at the required wave length (Figure S3, SM).

Acknowledgment: We thank Jussi Toppari, Johannes Feist and Ruth Tichauer for fruitful discussions. We thank Arpan Dutta for sharing the absorption spectrum of HBQ in PMMA and Dmitry Morozov for computing the potential energy profiles of proton transfer in HBQ. We thank the Center for Scientific Computing (CSC-IT Center for Science) for very generous computer resources.

Research funding: This work was supported by the Academy of Finland (DOI: 10.13039/501100002341, Grants 323996 and 332743).

Author contributions: G.G. acquired funding; I.S and G.G. performed the Molecular Dynamics simulations. I.S. analysed the data and prepared the figures; G.G. drafted the manuscript, which both authors revised

and edited. Both authors have accepted responsibility for the entire content of this manuscript and approved its submission.

Conflict of interest: The authors state no conflict of interest.

Data availability statement: The datasets generated and/or analyzed during the current study are available from the corresponding author upon reasonable request.

References

- [1] O. V. Mikhnenko, P. W. M. Blom, and T.-Q. Nguyen, "Exciton diffusion in organic semiconductors," *Energy Environ. Sci.*, vol. 8, pp. 1867–1888, 2015.
- [2] J. B. Aladekomo, S. Arnold, and M. Pope, "Triplet exciton diffusion and double photon absorption in tetracene," *Phys. Status Solidi*, vol. 80, pp. 333–340, 1977.
- [3] G. M. Akselrod, P. B. Deotare, N. J. Thompson, J. Lee, W. A. Tisdale, M. A. B. V. M. Menon, and V. Bulovic, "Visualization of exciton transport in ordered and disordered molecular solids," *Nat. commun.*, vol. 5, p. 3646, 2014.
- [4] A. Sneyd, T. Fukui, D. Palaček, S. Prodhon, Y. Wagner, Y. Zhang, J. Sung, S. Collins, T. Slater, Z. Andajji-Garmaroudi, L. MacFarlane, J. Garcia-Hernandez, L. Wang, G. Whittell, J. Hodgkiss, K. Chen, D. Beljonne, I. Manners, R. Friend, and A. Rao, "Efficient energy transport in an organic semiconductor mediated by transient exciton delocalization," *Sci. Adv.*, vol. 7, p. eabh4232, 2021.
- [5] F. F. Kong, X. J. Tian, Y. Zhang, Y. Zhang, G. Chen, Y. J. Yu, S. H. Jing, H. Y. Gao, Y. Luo, J. L. Yang, Z. C. Dong, and J. G. Hou, "Wavelike electronic energy transfer in donor-acceptor molecular systems through quantum coherence," *Nat. Nanotechnol.*, vol. 17, pp. 729–736, 2022.
- [6] A. J. Sneyd, D. Beljonne, and A. Rao, "A new frontier in exciton transport: Transient delocalization," *J. Chem. Phys. Lett.*, vol. 13, pp. 6820–6830, 2022.
- [7] S. Stäter, F. A. Wenzel, H. Welz, K. Kreger, J. Köhler, H.-W. Schmidt, and R. Hildner, "Directed gradients in the excited-state energy landscape of poly(3-hexylthiophene) nanofibers," *J. Am. Chem. Soc.*, vol. 145, pp. 13780–13787, 2023.
- [8] G. Lerario, D. Ballarini, A. Fieramosca, A. Cannavale, A. Genco, F. Mangione, S. Gambino, L. Dominici, M. D. Giorgi, G. Gigli, and D. Sanvitto, "High-speed flow of interacting organic polaritons," *Light Sci. Appl.*, vol. 6, p. e16212, 2017.
- [9] G. G. Rozenman, K. Akulov, A. Golombek, and T. Schwartz, "Long-range transport of organic exciton-polaritons revealed by ultrafast microscopy," *ACS Photonics*, vol. 5, pp. 105–110, 2018.
- [10] S. Hou, M. Khatoniar, K. Ding, Y. Qu, A. Napolov, V. M. Menon, and S. R. Forrest, "Ultralong-range energy transport

- in a disordered organic semiconductor at room temperature via coherent exciton-polariton propagation," *Adv. Mater.*, vol. 32(28), p. 2002127, 2020.
- [11] R. Pandya, R. Y. S. Chen, Q. Gu, J. Sung, C. Schneidermann, O. S. Ojambati, R. Chikkaraddy, J. Gorman, G. Jacucci, O. D. Onelli, T. Willhammar, D. N. Johnston, S. M. Collins, P. A. Midgley, F. Auras, T. Baikie, R. Jayaprakash, F. Mathevet, R. Soucek, M. Du, A. M. Alvertis, A. Ashoka, S. Vignolini, D. G. Lidzey, J. J. Baumberg, R. H. Friend, T. Barisien, L. Legrand, A. W. Chin, J. Yuen-Zhou, S. K. Saikin, P. Kukura, A. J. Musser, and A. Rao, "Microcavity-like exciton-polaritons can be the primary photoexcitation in bare organic semiconductors," *Nat. Commun.*, vol. 12, p. 6519, 2021.
- [12] M. Wurdack, E. Estrecho, S. Todd, T. Yun, M. Pieczarka, S. K. Earl, J. A. Davis, C. Schneider, A. G. Truscott, and E. A. Ostrovskaya, "Motional narrowing, ballistic transport, and trapping of room-temperature exciton polaritons in an atomically-thin semiconductor," *Nat. commun.*, vol. 12, p. 5366, 2021.
- [13] M. A. Berghuis, R. H. Tichauer, L. de Jong, I. Sokolovskii, P. Bai, M. Ramezani, S. Murai, G. Groenhof, and J. G. Rivas, "Controlling exciton propagation in organic crystals through strong coupling to plasmonic nanoparticle arrays," *ACS Photonics*, vol. 9, p. 123, 2022.
- [14] R. Pandya, A. Ashoka, K. Georgiou, J. Sung, R. Jayaprakash, S. Renken, L. Gai, Z. Shen, A. Rao, and A. J. Musser, "Tuning the coherent propagation of organic exciton-polaritons through dark state delocalization," *Adv. Sci.*, vol. 9, p. 2105569, 2022.
- [15] D. Xu, A. Mandal, J. M. Baxter, S.-W. Cheng, I. Lee, H. Su, S. Liu, D. R. Reichman, and M. Delor, "Ultrafast imaging of coherent polariton propagation and interactions," *Nat. commun.*, vol. 14, p. 3881, 2023.
- [16] M. Balasubrahmaniam, A. Simkovich, A. Golombek, G. Ankonina, and T. Schwartz, "Unveiling the mixed nature of polaritonic transport: From enhanced diffusion to ballistic motion approaching the speed of light," *Nat. Mater.*, vol. 22, p. 338–344, 2023.
- [17] K. J. Vahala, "Optical microcavities," *Nature*, vol. 424, pp. 839–846, 2003.
- [18] V. M. Agranovich and Y. N. Gartstein, "Nature and dynamics of low-energy exciton polaritons in semiconductor microcavities," *Phys. Rev. B*, vol. 75, p. 075302, 2007.
- [19] M. Litinskaya, "Propagation and localization of polaritons in disordered organic microcavities," *Phys. Lett. A*, vol. 372, pp. 3898–3903, 2008.
- [20] J. Feist and F. J. Garcia-Vidal, "Extraordinary exciton conductance induced by strong coupling," *Phys. Rev. Lett.*, vol. 114, p. 196402, 2015.
- [21] J. Schachenmayer, C. Genes, E. Tignone, and G. Pupillo, "Cavity enhanced transport of excitons," *Phys. Rev. Lett.*, vol. 114, p. 196403, 2015.
- [22] G. Engelhardt and J. Cao, "Polariton localization and dispersion properties of disordered quantum emitters in multimode microcavities," *Phys. Rev. Lett.*, vol. 130, p. 213602, 2023.
- [23] G. J. R. Aroeira, K. Kairys, and R. F. Ribeiro, "Theoretical analysis of exciton wave packet dynamics in polaritonic wires," *J. Phys. Chem. Lett.*, vol. 14, pp. 5681–5691, 2023.
- [24] P. Törmä and W. L. Barnes, "Strong coupling between surface plasmon polaritons and emitters: a review," *Rep. Prog. Phys.*, vol. 78, p. 013901, 2015.
- [25] M. S. Rider and W. L. Barnes, "Something from nothing: linking molecules with virtual light," *Contemp. Phys.*, vol. 62, no. 4, pp. 217–232, 2022.
- [26] V. M. Agranovich, M. Litinskaia, and D. G. Lidzey, "Cavity polaritons in microcavities containing disordered organic semiconductors," *Phys. Rev. B*, vol. 67, p. 085311, 2003.
- [27] M. Litinskaya, P. Reineker, and V. M. Agranovich, "Fast polariton relaxation in strongly coupled organic microcavities," *J. Lumin.*, vol. 110, pp. 364–372, 2004.
- [28] L. A. Martínez-Martínez, E. Eizner, S. Kéna-Cohen, and J. Yuen-Zhou, "Triplet harvesting in the polaritonic regime: A variational polaron approach," *J. Chem. Phys.*, vol. 151, p. 054106, 2019.
- [29] P. Michetti and G. C. L. Rocca, "Polariton dynamics in disordered microcavities," *Physica E*, vol. 40, pp. 1926–1929, 2008.
- [30] R. F. Ribeiro, "Multimode polariton effects on molecular energy transport and spectral fluctuations," *Comm. Chem.*, vol. 5, p. 48, 2022.
- [31] T. Freixanet, B. Sermage, A. Tiberj, and R. Planel, "In-plane propagation of excitonic cavity polaritons," *Phys. Rev. B*, vol. 61, p. 7233, 2000.
- [32] D. M. Myers, S. Mukherjee, J. Beaumariage, and D. W. Snoke, "Polariton-enhanced exciton transport," *Phys. Rev. B*, vol. 98, p. 235302, 2018.
- [33] I. Sokolovskii, R. H. Tichauer, D. Morozov, J. Feist, and G. Groenhof, "Multi-scale molecular dynamics simulations of enhanced energy transfer in organic molecules under strong coupling," *arXiv*, p. 2209.07309, 2022.
- [34] R. H. Tichauer, I. Sokolovskii, and G. Groenhof, "Tuning coherent propagation of organic exciton-polaritons through the cavity q-factor," *arXiv*, vol. 2304.13123, 2023.
- [35] D. Wellnitz, G. Pupillo, and J. Schachenmayer, "Disorder enhanced vibrational entanglement and dynamics in polaritonic chemistry," *Comm. Phys.*, vol. 5, p. 120, 2022.
- [36] J. A. Hutchison, T. Schwartz, C. Genet, E. Devaux, and T. W. Ebbesen, "Modifying chemical landscapes by coupling to vacuum fields," *Angew. Chem. Int. Ed.*, vol. 51, pp. 1592–1596, 2012.
- [37] C. H. Kim and T. Joo, "Coherent excited state intramolecular proton transfer probed by time-resolved fluorescence," *Phys. Chem. Chem. Phys.*, vol. 11, pp. 10266–10269, 2009.
- [38] J. Lee, C. H. Kim, and T. Joo, "Active role of proton in excited state intramolecular proton transfer reaction," *J. Phys. Chem. A*, vol. 117, pp. 1400–1405, 2013.
- [39] G. M. Akselrod, E. R. Young, M. S. Bradley, and V. Bulović, "Lasing through a strongly-coupled mode by intra-cavity pumping," *Opt. Express*, vol. 21, pp. 12122–12128, 2013.
- [40] A. Cargioli, M. Lednev, L. Lavista, A. Camposeo, A. Sassella, D. Pisignano, A. Tredicucci, F. J. Garcia-Vidal, J. Feist, and L. Persano, "Active control of polariton-enabled long-range energy transfer," *arXiv*, p. 2310.04121, 2023.
- [41] H. L. Luk, J. Feist, J. J. Toppari, and G. Groenhof, "Multi-scale molecular dynamics simulations of polaritonic chemistry," *J. Chem. Theory Comput.*, vol. 13, pp. 4324–4335, 2017.

- [42] R. H. Tichauer, J. Feist, and G. Groenhof, "Multi-scale dynamics simulations of molecular polaritons: the effect of multiple cavity modes on polariton relaxation," *J. Chem. Phys.*, vol. 154, p. 104112, 2021.
- [43] J. del Pino, J. Feist, and F. J. Garcia-Vidal, "Quantum Theory of Collective Strong Coupling of Molecular Vibrations with a Microcavity Mode," *New J. Phys.*, vol. 17, no. 5, p. 053040, May 2015.
- [44] E. Eizner, L. A. Martínez-Martínez, J. Yuen-Shou, and S. Kéna-Cohen, "Inverting singlet and triplet excited states using strong light-matter coupling," *Sci. Adv.*, vol. 5, p. aax4482, 2019.
- [45] P. Hohenberg and W. Kohn, "Inhomogeneous electron gas," *Phys. Rev.*, vol. 136, pp. 864–871, 1964.
- [46] E. Runge and E. K. U. Gross, "Density-functional theory for time-dependent systems," *Phys. Rev. Lett.*, vol. 52, pp. 997–1000, 1984.
- [47] S. Hirata and M. Head-Gordon, "Time-dependent density functional theory within the tamm-dancoff approximation," *Chem. Phys. Lett.*, vol. 314, pp. 291–299, 1999.
- [48] A. D. Becke, "A new mixing of Hartree-Fock and local density-functional theories," *J. Chem. Phys.*, vol. 98, p. 1372, 1993.
- [49] T. Yanai, D. P. Tew, and N. C. Handy, "A new hybrid exchange-correlation functional using the coulomb-attenuating method (cam-b3lyp)," *Chem. Phys. Lett.*, vol. 393, pp. 51–57, 2004.
- [50] R. Ditchfield, W. J. Hehre, and J. A. Pople, "Self-consistent molecular-orbital methods. ix. an extended gaussian-type basis for molecular-orbital studies of organic molecules," *J. Chem. Phys.*, vol. 54, pp. 724–728, 1971.
- [51] B. A. C. Horta, P. T. Merz, P. F. J. Fuchs, J. Dolenc, S. Riniker, and P. H. Hünenberger, "A gromos-compatible force field for small organic molecules in the condensed phase: The 2016h66 parameter set," *J. Chem. Theory Comput.*, vol. 12, pp. 3825–3850, 2016.
- [52] V. N. Staroverov, G. E. Scuseria, J. Tao, and J. P. Perdew, "Comparative assessment of a new nonempirical density functional: Molecules and hydrogen-bonded complexes," *J. Chem. Phys.*, vol. 119, no. 23, pp. 12 129–12 137, 2003.
- [53] D. Picconi, "Nonadiabatic quantum dynamics of the coherent excited state intramolecular proton transfer of 10-hydroxybenzo [h] quinoline," *Photochem. Photobiol. Sci.*, vol. 20, pp. 1455–1473, 2021.
- [54] M. E. Casida, C. Jamorski, K. C. Casida, and D. R. Salahub, "Molecular excitation energies to high-lying bound states from time-dependent density-functional response theory: Characterization and correction of the time-dependent local density approximation ionization threshold," *J. Chem. Phys.*, vol. 108, pp. 4439–4449, 1998.
- [55] A. D. Becke, "Density-functional thermochemistry. v. systematic optimization of exchange-correlation functionals," *J. Chem. Phys.*, vol. 107, pp. 8554–8560, 1997.
- [56] W. L. Jorgensen, J. Chandrasekhar, J. D. Madura, R. W. Impey, and M. L. Klein, "Comparison of simple potential functions for simulating liquid water," *J. Chem. Phys.*, vol. 79, pp. 926–935, 1983.
- [57] P. Michetti and G. C. L. Rocca, "Polariton states in disordered organic microcavities," *Phys. Rev. B.*, vol. 71, p. 115320, 2005.
- [58] T. Schwartz, J. A. Hutchison, J. Leonard, C. Genet, S. Haacke, and T. W. Ebbesen, "Polariton dynamics under strong light-molecule coupling," *ChemPhysChem*, vol. 14, pp. 125–131, 2013.
- [59] I. S. Ulusoy and O. Vendrell, "Dynamics and spectroscopy of molecular ensembles in a lossy microcavity," *J. Chem. Phys.*, vol. 153, p. 044108, 2020.
- [60] P. Antoniou, F. Suchanek, J. F. Varner, and J. J. Foley IV, "Role of cavity losses on nonadiabatic couplings and dynamics in polaritonic chemistry," *J. Phys. Chem. Lett.*, vol. 11, pp. 9063–9069, 2020.
- [61] S. Felicetti, J. Fregoni, T. Schnappinger, S. Reiter, R. de Vivie-Riedle, and J. Feist, "Photoprotecting uracil by coupling with lossy nanocavities," *J. Chem. Phys. Lett.*, vol. 11, pp. 8810–8818, 2020.
- [62] D. Hu, A. Mandal, B. M. Weight, and P. Huo, "Quasi-adiabatic propagation scheme for simulating polariton chemistry," *J. Chem. Phys.*, vol. 157, p. 194109, 2022.
- [63] G. Groenhof, C. Climent, J. Feist, D. Morozov, and J. J. Toppari, "Tracking polariton relaxation with multiscale molecular dynamics simulations," *J. Chem. Phys. Lett.*, vol. 10, pp. 5476–5483, 2019.
- [64] R. H. Tichauer, D. Morozov, I. Sokolovskii, J. J. Toppari, and G. Groenhof, "Identifying vibrations that control non-adiabatic relaxation of polaritons in strongly coupled molecule-cavity systems," *J. Phys. Chem. Lett.*, vol. 13, pp. 6259–6267, 2022.

Supplementary Material
for
Photochemical Initiation of Polariton
Propagation

Ilia Sokolovskii and Gerrit Groenhof*

*Nanoscience Center and Department of Chemistry, University of Jyväskylä, P.O. Box 35, 40014
Jyväskylä, Finland.*

E-mail: gerrit.x.groenhof@ju.fi

Contents

1	Molecular Dynamics Simulation Model	3
1.1	Multiscale Tavis-Cummings Hamiltonian	3
1.2	One-dimensional Periodic Cavity	4
1.3	Ehrenfest dynamics	7
2	Simulation details	8
2.1	HBQ model	8
2.2	Methylene Blue model	9
2.3	HBQ/MeB cavity simulations	12
3	Simulation Analysis	13
3.1	Monitoring exciton dynamics in the strong coupling regime	13
3.2	Photo-Absorption Spectra	13
3.2.1	Molecular absorption spectra	13
3.2.2	Cavity absorption spectra	14
4	Additional Results	15
4.1	Transparency of cavity mirrors	15
4.2	Potential energy surface of HBQ	16
4.3	Delayed exciton transport when HBQ reacts later	17
5	Animations	18
6	References	19

1 Molecular Dynamics Simulation Model

1.1 Multiscale Tavis-Cummings Hamiltonian

Within the single-excitation subspace, which is probed experimentally under weak driving conditions, and employing the rotating wave approximation (RWA), which is valid for light-matter coupling strengths below 10% of the material excitation energy,¹ the interaction between N molecules and n_{mode} confined light modes in a one-dimensional (1D) Fabry-Pérot cavity (Figure S1) is modelled with the multi-scale Molecular Dynamics (MD) extension of the traditional Tavis-Cummings model of quantum optics.²⁻⁵

$$\begin{aligned} \hat{H}^{\text{TC}} = & \sum_j^N h\nu_j(\mathbf{R}_j) \hat{\sigma}_j^+ \hat{\sigma}_j^- + \sum_{k_z}^{n_{\text{mode}}} \hbar\omega_{\text{cav}}(k_z) \hat{a}_{k_z}^\dagger \hat{a}_{k_z} + \\ & \sum_j^N \sum_{k_z}^{n_{\text{mode}}} \hbar g_j(k_z) \left(\hat{\sigma}_j^+ \hat{a}_{k_z} e^{ik_z z_j} + \hat{\sigma}_j^- \hat{a}_{k_z}^\dagger e^{-ik_z z_j} \right) + \\ & \sum_i^N V_{S_0}^{\text{mol}}(\mathbf{R}_i) \end{aligned} \quad (1)$$

Here, $\hat{\sigma}_j^+$ ($\hat{\sigma}_j^-$) is the operator that excites (de-excites) molecule j from the electronic ground (excited) state $|S_0^j(\mathbf{R}_j)\rangle$ ($|S_1^j(\mathbf{R}_j)\rangle$) to the electronic excited (ground) state $|S_1^j(\mathbf{R}_j)\rangle$ ($|S_0^j(\mathbf{R}_j)\rangle$); \mathbf{R}_j is the vector of the Cartesian coordinates of all atoms in molecule j , centered at z_j ; \hat{a}_{k_z} ($\hat{a}_{k_z}^\dagger$) is the annihilation (creation) operator of an excitation of a cavity mode with wave-vector k_z ; $h\nu_j(\mathbf{R}_j)$ is the excitation energy of molecule j , defined as:

$$h\nu_j(\mathbf{R}_j) = V_{S_1}^{\text{mol}}(\mathbf{R}_j) - V_{S_0}^{\text{mol}}(\mathbf{R}_j) \quad (2)$$

with $V_{S_0}^{\text{mol}}(\mathbf{R}_j)$ and $V_{S_1}^{\text{mol}}(\mathbf{R}_j)$ the adiabatic potential energy surfaces (PESs) of molecule j in the electronic ground (S_0) and excited (S_1) state, respectively. The last term in Equation 1 is the total potential energy of the system in the absolute ground state (*i.e.*, with no excitations in neither the molecules nor the cavity modes), defined as the sum of the ground-state potential energies of all

molecules in the cavity. The $V_{S_0}^{\text{mol}}(\mathbf{R}_j)$ and $V_{S_1}^{\text{mol}}(\mathbf{R}_j)$ adiabatic PESs are modelled at the hybrid quantum mechanics / molecular mechanics (QM/MM) level of theory.^{6,7}

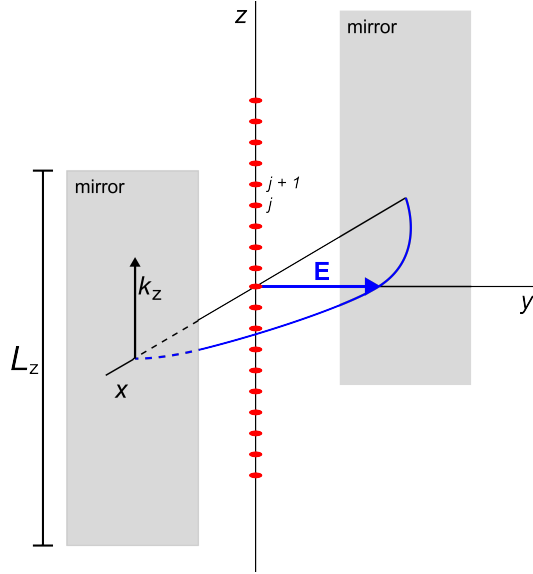


Figure S1: One-dimensional (1D) Fabry-Pérot micro-cavity model. Two reflecting mirrors located at $-\frac{1}{2}x$ and $\frac{1}{2}x$, confine light modes along this direction, while free propagation along the z direction is possible for plane waves with in-plane momentum k_z and energy $\hbar\omega_{\text{cav}}(k_z)$. The vacuum field vector (red) points along the y -axis, reaching a maximum amplitude at $x = 0$ where the N molecules (magenta ellipses) are placed, distributed along the z -axis at positions z_j with $1 \leq j \leq N$.

The third term in Equation 1 describes the light-matter interaction within the dipolar approximation through $g_j(k_z)$:

$$g_j(k_z) = -\boldsymbol{\mu}_j^{\text{TDM}}(\mathbf{R}_j) \cdot \mathbf{u}_{\text{cav}} \sqrt{\frac{\hbar\omega_{\text{cav}}(k_z)}{2\epsilon_0 V_{\text{cav}}}} \quad (3)$$

where $\boldsymbol{\mu}_j^{\text{TDM}}(\mathbf{R}_j)$ is the transition dipole moment of molecule j that depends on the molecular geometry (\mathbf{R}_j); \mathbf{u}_{cav} the unit vector in the direction of the electric component of cavity vacuum field (*i.e.*, $|\mathbf{E}| = \sqrt{\hbar\omega_{\text{cav}}(k_z)/2\epsilon_0 V_{\text{cav}}}$), here along the y -direction (Figure S1); ϵ_0 the vacuum permittivity; and V_{cav} the cavity mode volume.

1.2 One-dimensional Periodic Cavity

Following Michetti and La Rocca,⁴ we impose periodic boundary conditions in the z -direction of our cavity, and thus restrict the wave vectors, k_z , to discrete values: $k_{z,p} = 2\pi p/L_z$ with $p \in \mathbb{Z}$ and

L_z the length of the 1D cavity. With this approximation the molecular Tavis-Cummings Hamiltonian in Equation 1 can be represented as an $(N + n_{\text{mode}})$ by $(N + n_{\text{mode}})$ matrix with four blocks:⁵

$$\mathbf{H}^{\text{TC}} = \begin{pmatrix} \mathbf{H}^{\text{mol}} & \mathbf{H}^{\text{int}} \\ \mathbf{H}^{\text{int}\dagger} & \mathbf{H}^{\text{cav}} \end{pmatrix} \quad (4)$$

We compute the elements of this matrix in the product basis of adiabatic molecular states times cavity mode excitations:

$$\begin{aligned} |\phi_j\rangle &= \hat{\sigma}_j^+ |\mathbf{S}_0^1 \mathbf{S}_0^2 \dots \mathbf{S}_0^{N-1} \mathbf{S}_0^N\rangle \otimes |00\dots 0\rangle \\ &= \hat{\sigma}_j^+ |\Pi_i^N \mathbf{S}_0^i\rangle \otimes |\Pi_k^{n_{\text{mode}}} 0_k\rangle \\ &= \hat{\sigma}_j^+ |\phi_0\rangle \end{aligned} \quad (5)$$

for $1 \leq j \leq N$, and

$$\begin{aligned} |\phi_{j>N}\rangle &= \hat{a}_{j-N}^\dagger |\mathbf{S}_0^1 \mathbf{S}_0^2 \dots \mathbf{S}_0^{N-1} \mathbf{S}_0^N\rangle \otimes |00\dots 0\rangle \\ &= \hat{a}_{j-N}^\dagger |\Pi_i^N \mathbf{S}_0^i\rangle \otimes |\Pi_k^{n_{\text{mode}}} 0_k\rangle \\ &= \hat{a}_{j-N}^\dagger |\phi_0\rangle \end{aligned} \quad (6)$$

for $N < j \leq N + n_{\text{mode}}$. In these expressions $|00\dots 0\rangle$ indicates that the Fock states for all n_{mode} cavity modes are empty. The basis state $|\phi_0\rangle$ is the ground state of the molecule-cavity system with no excitations of neither the molecules nor cavity modes:

$$|\phi_0\rangle = |\mathbf{S}_0^1 \mathbf{S}_0^2 \dots \mathbf{S}_0^{N-1} \mathbf{S}_0^N\rangle \otimes |00\dots 0\rangle = |\Pi_i^N \mathbf{S}_0^i\rangle \otimes |\Pi_k^{n_{\text{mode}}} 0_k\rangle \quad (7)$$

The upper left block, \mathbf{H}^{mol} , is an $N \times N$ matrix containing the single-photon excitations of the molecules. Because we neglect direct excitonic interactions between molecules, this block is

diagonal, with elements labeled by the molecule indices j :

$$H_{j,j}^{\text{mol}} = \langle \phi_0 | \hat{\sigma}_j \hat{H}^{\text{TC}} \hat{\sigma}_j^\dagger | \phi_0 \rangle \quad (8)$$

for $1 \leq j \leq N$. Each matrix element of \mathbf{H}^{mol} thus represents the potential energy of a molecule, j , in the electronic excited state $|S_1^j(\mathbf{R}_j)\rangle$ while all other molecules, $i \neq j$, are in the electronic ground state $|S_0^i(\mathbf{R}_i)\rangle$:

$$H_{j,j}^{\text{mol}} = V_{S_1}^{\text{mol}}(\mathbf{R}_j) + \sum_{i \neq j}^N V_{S_0}^{\text{mol}}(\mathbf{R}_i) \quad (9)$$

The lower right block, \mathbf{H}^{cav} , is an $n_{\text{mode}} \times n_{\text{mode}}$ matrix (with $n_{\text{mode}} = n_{\text{max}} - n_{\text{min}} + 1$) containing the single-photon excitations of the cavity modes, and is also diagonal:

$$H_{p,p}^{\text{cav}} = \langle \phi_0 | \hat{a}_p \hat{H}^{\text{TC}} \hat{a}_p^\dagger | \phi_0 \rangle \quad (10)$$

for $n_{\text{min}} \leq p \leq n_{\text{max}}$. Here, \hat{a}_p^\dagger excites cavity mode p with wave-vector $k_{z,p} = 2\pi p/L_z$. In these matrix elements, all molecules are in the electronic ground state (S_0). The energy is therefore the sum of the cavity energy at $k_{z,p}$, and the molecular ground state energies:

$$H_{p,p}^{\text{cav}} = \hbar\omega_{\text{cav}}(2\pi p/L_z) + \sum_j^N V_{S_0}^{\text{mol}}(\mathbf{R}_j) \quad (11)$$

where, $\omega_{\text{cav}}(k_{z,p})$ is the cavity dispersion (dashed curve in Figure 1f, main text):

$$\omega_{\text{cav}}(k_{z,p}) = \sqrt{\omega_0^2 + c^2 k_{z,p}^2 / n^2} \quad (12)$$

with $\hbar\omega_0$ the energy at $k_0 = 0$, n the refractive index of the medium and c the speed of light in vacuum.

The two $N \times n_{\text{mode}}$ off-diagonal blocks \mathbf{H}^{int} and $\mathbf{H}^{\text{int}\dagger}$ in the multi-mode Tavis-Cummings Hamiltonian (Equation 4) model the light-matter interactions between the molecules and the cavity modes. Within the long-wavelength approximation these matrix elements can be approximated by

the overlap between the transition dipole moment of molecule j and the transverse electric field of cavity mode p at the geometric center z_j of that molecule:

$$\begin{aligned}
H_{j,p}^{\text{int}} &= -\boldsymbol{\mu}_j^{\text{TDM}}(\mathbf{R}_j) \cdot \mathbf{u}_{\text{cav}} \sqrt{\frac{\hbar\omega_{\text{cav}}(2\pi p/L_z)}{2\epsilon_0 V_{\text{cav}}}} \langle \phi_0 | \hat{\sigma}_j \hat{\sigma}_j^\dagger \hat{a}_p e^{i2\pi p z_j / L_z} \hat{a}_p^\dagger | \phi_0 \rangle \\
&= -\boldsymbol{\mu}_j^{\text{TDM}}(\mathbf{R}_j) \cdot \mathbf{u}_{\text{cav}} \sqrt{\frac{\hbar\omega_{\text{cav}}(2\pi p/L_z)}{2\epsilon_0 V_{\text{cav}}}} e^{i2\pi p z_j / L_z}
\end{aligned} \tag{13}$$

for $1 \leq j \leq N$ and $n_{\text{min}} \leq p \leq n_{\text{max}}$.

1.3 Ehrenfest dynamics

In our simulations classical trajectories evolve under the influence of the expectation value of forces with respect to the polaritonic wave function,⁸ while the polaritonic wave function evolves along with the classical degrees of freedom. By expanding the total wave function as a linear combination of the *time-independent* diabatic light-matter states (Equations 5 and 6):

$$|\Psi(t)\rangle = \sum_j^{N+n_{\text{modes}}} |\phi_j\rangle c_j(t) \tag{14}$$

the evolution of the *time-dependent* diabatic expansion coefficients, $c_j(t)$, is obtained by numerically integrating the Schrödinger equation over discrete time intervals, Δt .

$$\mathbf{c}(t + \Delta t) = \mathbf{P}^{\text{dia}} \mathbf{c}(t) \tag{15}$$

Here, $\mathbf{c}(t)$ is a vector containing the diabatic expansion coefficients $c_j(t)$ and \mathbf{P}^{dia} the propagator in the diabatic basis

$$\mathbf{P}^{\text{dia}} = \exp \left[-i \left(\mathbf{H}^{\text{TC}}(t + \Delta t) + \mathbf{H}^{\text{TC}}(t) - i\hbar\gamma \right) \Delta t / 2\hbar \right] \tag{16}$$

To account for the losses due to photon-leakage through the imperfect cavity mirrors, we add the decay rates of the cavity modes to the Tavis-Cummings Hamiltonian, here represented as a diagonal matrix, γ , with the cavity mode decay rates γ_k as elements.⁹⁻¹² Because of these decay terms, the norm of the total wave function, $|\Psi(t)|^2 = \sum_j^{N+n_{\text{modes}}} |c_j|^2$, is not conserved but decreases due to the losses.

2 Simulation details

2.1 HBQ model

The Gromos-2016H66 force field was used to model the interactions, because it contains a validated cyclohexane model,¹³ which was used as the solvent for HBQ in our simulations. In this united-atom representation of cyclohexane, none of the atoms carries a partial charge. Because HBQ was kept frozen during the solvent equilibration and modeled at the QM level in all other simulations, there was no need for assigning partial charges to the HBQ atoms. The Gromos96 atom-types used for HBQ to model the Van der Waals interactions with the cyclohexane solvent, are HC for all aromatic hydrogen atoms, C for all carbon atoms, NR for the aromatic nitrogen atom, OA for the hydroxyl oxygen atom and H for the hydroxyl proton.

One HBQ molecule was geometry-optimized and placed inside a rectangular box that was subsequently filled with 402 cyclohexane molecules. The simulation box, which thus contained 2436 atoms, was equilibrated for 100 ns. During equilibration, the coordinates of the HBQ atoms were kept fixed. The LINCS algorithm was used to constrain bond lengths in cyclohexane,¹⁴ enabling a time step of 2 fs. Temperature and pressure were maintained at 300 K and 1 atmosphere by means of weak-coupling to an external bath ($\tau_T = 0.1$ ps, $\tau_P = 1$ ps).¹⁵ The Lennard-Jones potential was truncated at 1.4 nm.

Snapshots were extracted from the equilibration trajectory and further equilibrated for 50 ps at the QM/MM level with a time step of 1 fs. In these QM/MM simulations HBQ was modelled with density functional theory (DFT), using the CAM-B3LYP functional,¹⁶⁻¹⁸ in combination with

a 3-21G basis set.¹⁹ The cyclohexane solvent was described with the 2016H66 parameter set of the Gromos96 force field.¹³ The QM subsystem was mechanically embedded within the MM subsystem. Because cyclohexane atoms are uncharged, the interactions between the QM and MM regions were modeled with Lennard-Jones potentials only. We used time-dependent DFT (TD-DFT),²⁰ within the Tamm-Dancoff approximation (TDA),²¹ in combination with the CAM-B3LYP functional and the 3-21G basis set, to model the singlet excited electronic (S_1) state of HBQ. All QM/MM simulations of HBQ outside of the cavity were performed with GROMACS version 4.5.3,²² using the QM/MM interface to TeraChem version 1.93.^{23,24}

2.2 Methylene Blue model

The Amber03 force field was used to model the interactions between Methylene Blue (MeB) and the water solvent, which was described with the TIP3P water model.²⁵ Atom types and partial charges for the MeB atoms (Figure S2) are listed in Table S1. The partial charges of the atoms were derived following the procedure recommended for the Amber03 force field.^{26,27} First, the geometry of MeB was minimized at the HF/6-31G** level of *ab initio* theory, using the IEFPCM continuum solvent model with a relative dielectric constant of 4.0.²⁸ After the geometry optimizations, the electrostatic potential at 10 concentric layers of 17 points per unit area around each atom was evaluated using the electron density calculated at the B3LYP/cc-pVTZ level of DFT theory,¹⁶ again using the IEFPCM continuum solvent model with a relative dielectric constant of 4.0.²⁸ The atomic charges were obtained by performing a two-stage RESP fit to the electrostatic potential,²⁷ the first without symmetry constraints, and the second with symmetry constraints on chemically identical atoms.

A single MeB molecule was geometry-optimized at the B97/3-21G level of theory and placed at the center of a rectangular box that was filled with 2031 TIP3P water molecules.²⁵ A 1.0 nm cut-off was used for the Van der Waals' interactions, which were modeled with Lennard-Jones potentials, while the Coulomb interactions were computed with the smooth particle mesh Ewald method,²⁹ using a 1.0 nm real space cut-off and a grid spacing of 0.12 nm and a relative tolerance at the real

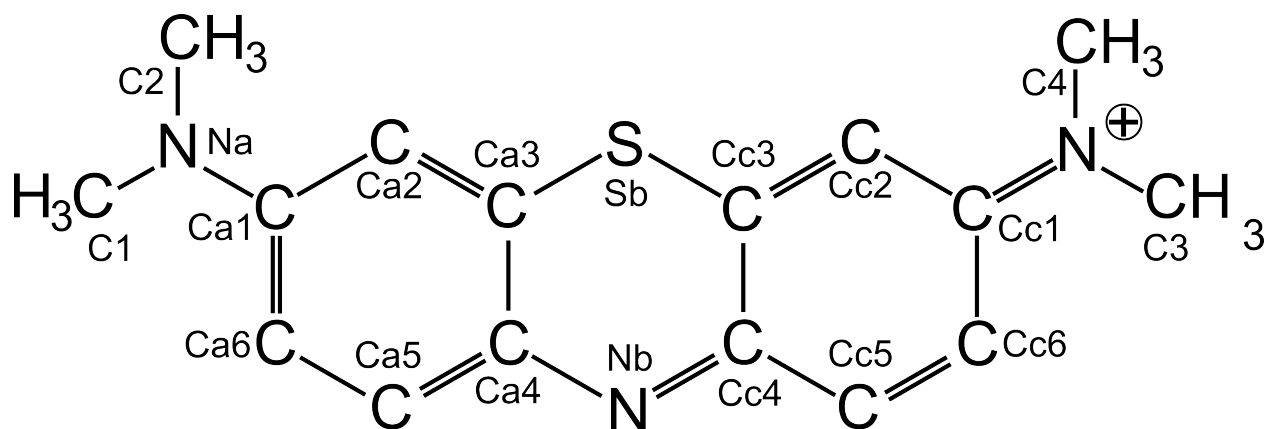


Figure S2: Structure and atom names of Methylene Blue. Not all hydrogens are shown, but their names take the name of the carbon atom plus an integer, *e.g.* HA2 is attached to CA2 and H21, H22 and H23 are attached to carbon C2.

space cut-off of 10^{-5} . The simulation box, containing 6,131 atoms, was equilibrated for 1 ns at the force field level of theory. During this equilibration, the coordinates of the MeB atoms were kept fixed. The temperature was kept at 300 K with the v-rescale thermostat,³⁰ while the pressure was kept constant at 1 atmosphere using the Berendsen isotropic pressure coupling algorithm,¹⁵ with a time constant of 1 ps. The SETTLE algorithm was applied to constrain the internal degrees of freedom of water molecules,³¹ enabling a time step of 2 fs in the classical MD simulations.

After equilibration at the force field (MM) level, the system was further equilibrated at the QM/MM level for 10 ps. The time step was reduced to 1 fs. The Methylene Blue molecule was modelled at the DFT level, using the B97 functional,³² in combination with the 3-21G basis set.¹⁹ The water solvent was modelled with the TIP3P force field.²⁵ The QM system experienced the Coulomb field of all MM atoms within a 1.0 nm cut-off sphere and Lennard-Jones interactions between MM and QM atoms were added. The singlet electronic excited state (S_1) was modeled with TD-DFT,²⁰ using the B97 functional in combination with the 3-21G basis set for the QM region (*i.e.*, TD-B97/3-21G),¹⁹. At this level of QM/MM theory, the excitation energy is 2.5 eV. The overestimation of the vertical excitation energy is due to the limited accuracy of the employed level of theory, but was compensated by adding an off-set to the cavity resonance energy (see subsection 2.3). The QM/MM simulations were performed with GROMACS version 4.5.3,²² interfaced to TeraChem version 1.93.^{23,24}

Table S1: Amber03 atomtypes and partial charges for Methylene Blue. Atom names are defined in Figure S2.

name	type	charge (e)
Ca1	CA	0.054312
Na	NA	0.154719
C1	CT	-0.284923
H11	H1	0.128201
H12	H1	0.128201
H13	H1	0.128201
C2	CT	-0.275632
H21	H1	0.127095
H22	H1	0.127095
H23	H1	0.127095
Ca2	CA	-0.205067
Ha2	HA	0.181067
Ca3	C	-0.101342
Ca4	CA	0.624779
Ca5	CA	-0.286158
Ha5	HA	0.187369
Ca6	CA	-0.141958
Ha6	HA	0.158598
Nb	NB	-0.712421
Sb	S	0.049117
Cc1	CA	0.054312
Nc	NA	0.154719
C3	CT	-0.284923
H31	H1	0.128201
H32	H1	0.128201
H33	H1	0.128201
C4	CT	-0.275632
H41	H1	0.127095
H42	H1	0.127095
H43	H1	0.127095
Cc2	CA	-0.205067
Hc2	HA	0.181067
Cc3	C	-0.101342
Cc4	CA	0.624779
Cc5	CA	-0.286158
Hc5	HA	0.187369
Cc6	CA	-0.141958
Hc6	HA	0.158598

2.3 HBQ/MeB cavity simulations

From the HBQ QM/MM trajectory, we selected single HBQ snapshots, which we combined with 1023 Methylene Blue molecules from the MeB QM/MM trajectory. These 1024 molecules, including their solvent environments, were placed at equal inter-molecular separations on the z -axis of a 1D,⁴ 50 μm long, symmetric optical Fabry-Pérot micro-cavity. The dispersion of this cavity was modelled with 239 discrete modes (*i.e.*, $k_{z,p} = 2\pi p/L_z$ with $-119 \leq p \leq 119$ and $L_z = 50 \mu\text{m}$). The micro-cavity was red-detuned with respect to the Methylene Blue absorption maximum, which is 2.5 eV at the TD-B97/3-21G//Amber03 level of theory used in this work, such that the energy of the fundamental cavity mode at zero incidence angle ($k_0 = 0$) was $\hbar\omega_0 = 2.18 \text{ eV}$. To maximize the collective light-matter coupling strength, the transition dipole moments of all molecules were aligned to the vacuum field at the start of the simulation. With a vacuum field strength of $\mathbf{E}_y = 0.00004 \text{ (} 0.21 \text{ MVcm}^{-1}\text{)}$ this configuration yields a Rabi splitting of $\hbar\Omega^{\text{Rabi}} = 323 \text{ meV}$. All simulations were performed for a lossy cavity with a decay rate of $\hbar\gamma_{\text{cav}} = 0.04 \text{ eV}$ or $\gamma_{\text{cav}} = 66.7 \text{ ps}^{-1}$. At such rate, the lifetime, τ_{cav} , of the lossy cavity is comparable to the 2-14 fs lifetimes of metallic Fabry-Pérot cavities used in experiments on strong coupling with organic molecules.³³⁻³⁵ With a lifetime of 15 fs and a resonance at 2.18 eV, the Quality-factor, defined as $Q = \omega_{\text{cav}}\tau_{\text{cav}}$, would be 50 for our cavity. A leap-frog Verlet algorithm with a 0.5 fs time step was used to integrate the nuclear dynamics, while the unitary propagator in the diabatic basis was used to propagate the polaritonic degrees of freedom.³⁶ The simulation was performed with GROMACS version 4.5.3,²² in which the multi-mode Tavis-Cummings QM/MM model was implemented,⁵ in combination with Gaussian16.³⁷ The GROMACS source code is available for download from <https://github.com/upper-polariton/GMXTC>. The results presented in the main manuscript are averages over four trajectories, started with different initial conditions.

Because the molecules do not interact directly, but rather via the cavity modes, there are no issues in using different QM/MM descriptions for HBQ and MeB. Although the solvents as well as the force fields and QM methods were chosen because of convenience, we emphasize that for the purpose of this work it is not essential to have the most accurate description of the bare excitation

energies of the molecules, but rather to have a realistic model of the molecular degrees of freedom, including the solvent environment. We speculate that for practical realizations HBQ could be embedded via small micro-droplets of a suitable solvent within the polymer matrix containing MeB, or *vice versa*.

3 Simulation Analysis

3.1 Monitoring exciton dynamics in the strong coupling regime

To track the propagation of the excitonic wavepacket, we plotted the probability density of the excitonic contributions to the total time-dependent wave function $|\Psi(t)|^2$ at the positions of the molecules, z_j , as a function of time. We thus represent the density as a *discrete* distribution at grid points that correspond to the molecular positions, rather than a continuous distribution. The amplitude of the excitonic wave function, $|\Psi_{\text{exc}}(t)\rangle$, at position z_j in the 1D cavity (with $z_j = (j - 1)L_z/N$ for $1 \leq j \leq N$) is obtained by projecting the excitonic basis state in which molecule j at position z_j is excited ($|\phi_j\rangle = \hat{\sigma}_j^+|\phi_0\rangle$) to the total wave function (Equation 14):

$$|\Psi_{\text{exc}}(z_j, t)\rangle = \hat{\sigma}_j^+|\phi_0\rangle\langle\phi_0|\hat{\sigma}_j|\Psi(t)\rangle = c_j(t) \quad (17)$$

where the $c_j(t)$ is the time-dependent expansion coefficients of the total wave function $|\Psi(t)\rangle$ (Equation 14).

3.2 Photo-Absorption Spectra

3.2.1 Molecular absorption spectra

The absorption spectra of HBQ and MeB were computed from QM/MM trajectories in the ground (S_0) state. These spectra were composed of the S_1 - S_0 energy gaps by super-position of Gaussian

functions:³⁸

$$I_{\text{mol}}^{\text{abs}}(E) \propto \sum_i^s \Delta E_i \exp \left[-\frac{(E - \Delta E_i)^2}{2\sigma^2} \right] |\boldsymbol{\mu}_i^{\text{TDM}}|^2 \quad (18)$$

where $I_{\text{mol}}^{\text{abs}}(E)$ is the intensity of the molecular absorption as a function of excitation energy (E), s the number of snapshots included in the analysis, ΔE_i the excitation energy in snapshot i and $\boldsymbol{\mu}_i^{\text{TDM}}$ the transition dipole moment of that excitation. A width of $\sigma = 0.05$ eV was used for the convolution.

The emission spectrum of HBQ was computed from a 10 ps QM/MM trajectory in the excited (S_1) state. The first 100 fs were discarded to sample only the relaxed photo-product state. The spectra were composed as in Equation 18, using the S_1 - S_0 energy gaps and transition dipole moments from the trajectory. As for the absorption spectra, a width of $\sigma = 0.05$ eV was used for the convolution.

3.2.2 Cavity absorption spectra

To compute the absorption spectrum of the molecule-cavity system as a function of energy and k_z -vector, we first diagonalized the Tavis-Cummings Hamiltonian, using molecular energies and transition dipole moments from the equilibrium QM/MM simulations, to obtain the $N + n_{\text{mode}}$ hybrid light-matter states $|\psi^m\rangle$:^{4,39}

$$|\psi^m\rangle = \left(\sum_j^N \beta_j^m \hat{\sigma}_j^{\dagger} + \sum_p^{n_{\text{mode}}} \alpha_p^m \hat{a}_p^{\dagger} \right) |\phi_0\rangle \quad (19)$$

with eigenenergies E_m . The β_j^m and α_p^m expansion coefficients reflect the contribution of the molecular excitations ($|S_1^j(\mathbf{R}_j)\rangle$) and the cavity mode excitations ($|1_p\rangle$) to polariton $|\psi^m\rangle$.

Following Lidzey and coworkers,⁴⁰ we define the "visibility", I^m , of polaritonic state $|\psi^m\rangle$ as the total photonic contribution to that state (*i.e.*, $I^m \propto \sum_p^{n_{\text{max}}} |\alpha_p^m|^2$). Thus, for each frame of the MeB QM/MM trajectory, the polaritonic states were computed and the energy gaps of these states with respect to the overall ground state (*i.e.*, E^0 , with all molecules in S_0 , no photon in the cavity, Equation 7) were extracted for all cavity modes, p , and summed up into a superposition of Gaussian

functions, weighted by $|\alpha_p^m|^2$:

$$I^{\text{abs}}(E, k_{z,p}) \propto \sum_t^s \left[\sum_m^{N+n_{\text{max}}+1} |\alpha_{p,t}^m|^2 \exp\left[-\frac{(E - \Delta E_t^m)^2}{2\sigma^2}\right] \right] \quad (20)$$

Here, $I^{\text{abs}}(E, k_{z,p})$ is the absorption intensity as a function of excitation energy E and in-plane momentum $k_{z,p} = 2\pi p/L_z$, s the number of trajectory frames included in the analysis, ΔE_t^m the excitation energy of polaritonic state m in frame t (*i.e.*, $\Delta E_t^m = E_t^m - E_t^0$) and $\alpha_{p,t}^m$ the expansion coefficient of cavity mode p in polaritonic state m in that frame (equation 19). A width of $\sigma = 0.05$ eV was used for the convolution.

4 Additional Results

4.1 Transparency of cavity mirrors

The reflectivity of a hypothetical Farby-Pérot micro-cavity composed of a 20 nm silver mirror on top of a 167 nm acrylic polymer layer and deposited on a silver substrate, was computed with the "Reflectance Calculator" of Filmetrics® (<https://www.filmetrics.com/reflectance-calculator>) and plotted as a function of wavelength (black) in Figure S3, together with the absorption spectra of HBQ in polymethyl-methacrylate (PMMA) (blue),⁴¹ and of MeB in water (red). Because the zeroth-order cavity mode is resonant with the main absorption peak of MeB centered at 668 nm, the cavity is transparent around that wavelength. With a sufficiently high concentration of MeB in the polymer layer, this absorption peak will split into the LP and UP bands, separated by the Rabi splitting. Because the reflectivity of the top mirror is reduced by more than 50% at the absorption maxima of HBQ (375 nm and 360 nm), we anticipate that this mixed HBQ/MeB-cavity system will still have a significant cross-section for selectively exciting HBQ, and initiate the transport via the excited-state intra-molecular proton transfer process.

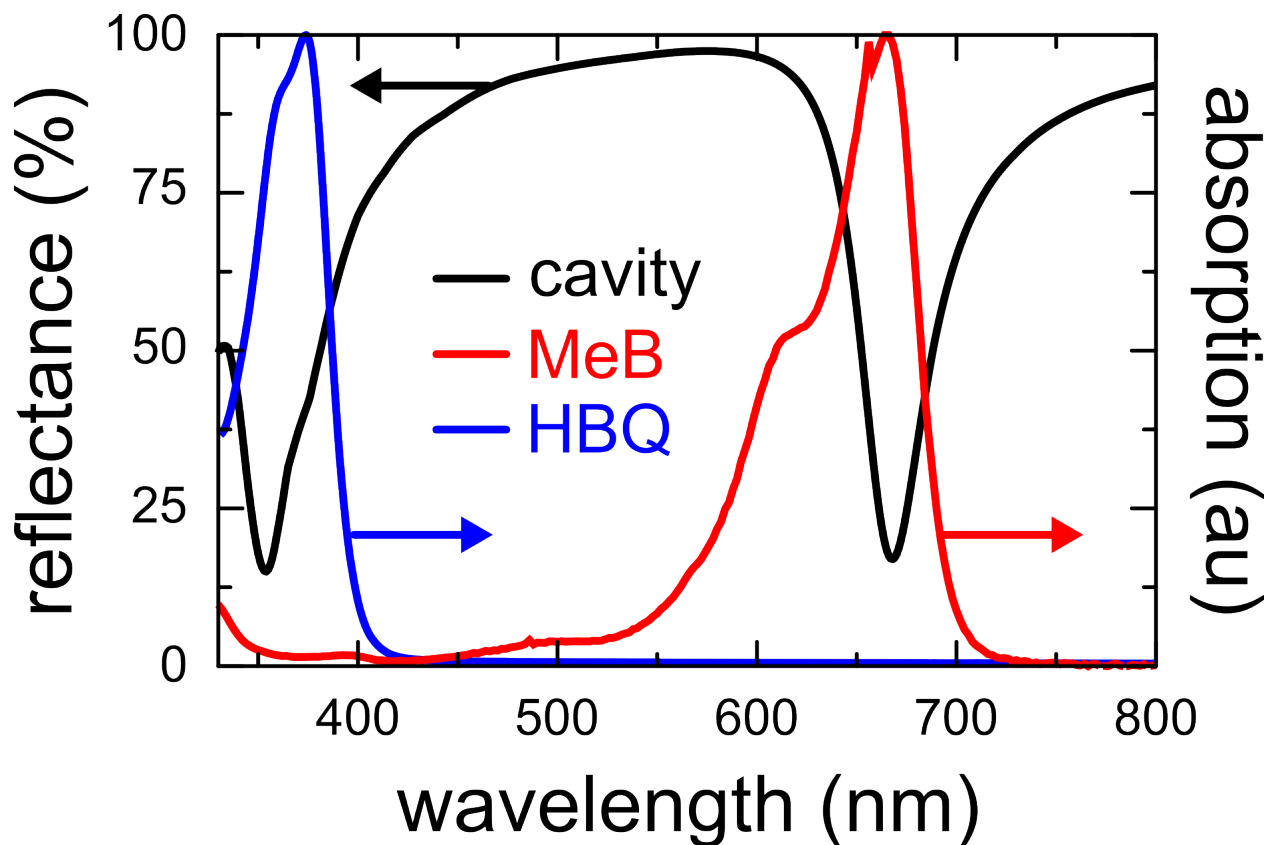


Figure S3: Calculated reflectance (black) spectrum of a Fabry-Pérot micro-cavity with a 20 nm silver mirror on top of a 167 nm polymer layer deposited on a silver substrate. Absorption spectra of MeB and HBQ are plotted in red and blue, respectively.

4.2 Potential energy surface of HBQ

In Figure S4 we compare the minimum energy potential energy profiles for the proton transfer reaction in the ground (S_0) and first excited electronic states (S_1) at the CAMB3LYP/3-21G,¹⁸ and TPSSh/cc-pVDZ levels of theory.⁴² These profiles were obtained by performing geometry optimizations on the S_1 potential energy surface at 33 equidistant points along the reaction coordinate, defined as the difference between the O-H and N-H distances (inset in Figure S4). The results of the scan suggest that the CAMB3LYP/3-21G model provides a potential energy surface on which proton transfer is barrierless in the excited state, in qualitative agreement with the calculations at the TPSSh/cc-pVDZ level of theory of Picconi,⁴³ that, in turn, are in good agreement with experiment.

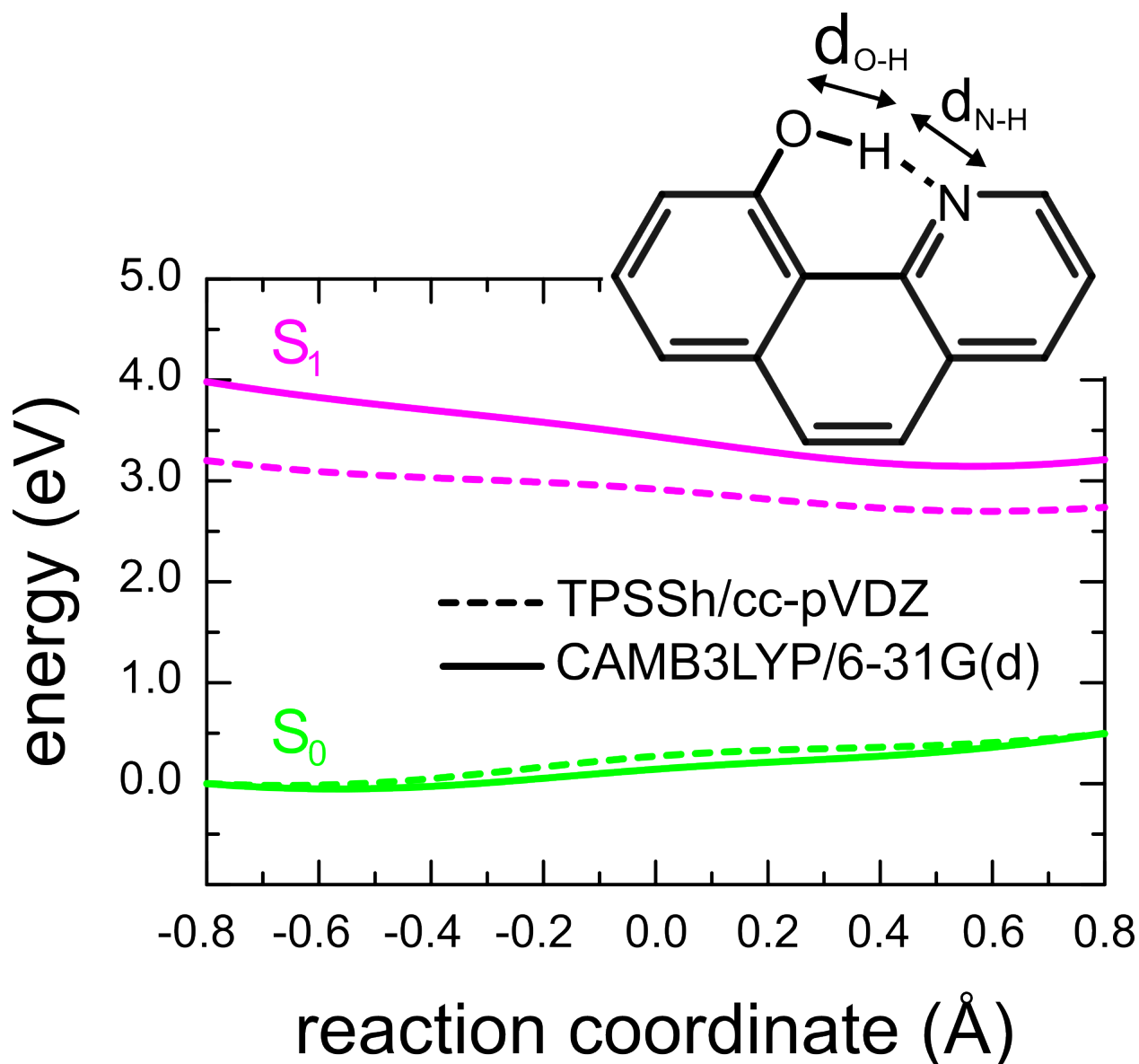


Figure S4: Minimum energy profile for excited-state intra-molecular proton transfer in HBQ as a function of the reaction coordinate defined as $d_{\text{O-H}} - d_{\text{N-H}}$ (inset) in the electronic ground state (S_0 , green) and excited state (S_1 , magenta) at the CAMB3LYP/3-21G (continuous lines) TPSSh/cc-pVDZ (dashed lines) levels of theory.

4.3 Delayed exciton transport when HBQ reacts later

In Figure S5 we show that when ES IPT occurs later, here 50 fs after photo-excitation, also the polariton-mediated exciton transport starts later.

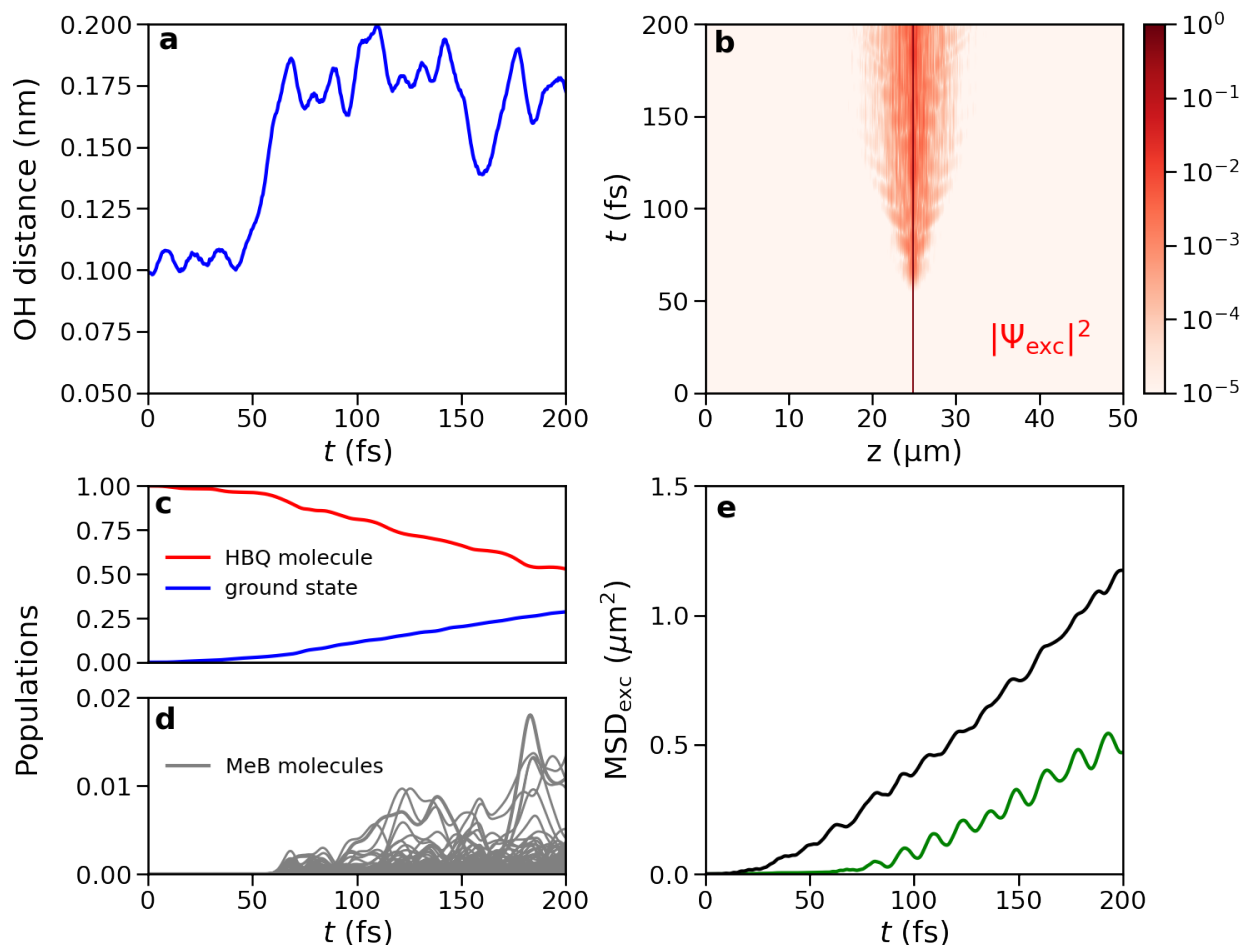


Figure S5: Delayed polariton-mediated exciton transport when the ESIPT in HBQ occurs later. Panel **a** shows the distance between the hydroxyl oxygen and proton, which we use as the reaction coordinate for the excited state proton transfer reaction as (Figure S4), a function of time after instantaneous excitation into the highest-energy eigenstate of the molecule-cavity system, which is dominated by the S_1 state of HBQ (*i.e.*, $|\beta_{\text{HBQ}}|^2 \approx 0.99$). Panel **b** shows the probability density of the excitonic part, $|\Psi_{\text{exc}}|^2$, of the total wavefunction as a function of the z -coordinate (horizontal axis) and time (vertical axis). Panels **c** and **d** show the contribution of the HBQ molecule (red) and Methylene Blue molecules (grey) to the total wavefunction, as well as the population of the ground state (blue). Panel **e** shows the Mean Squared Displacement (*i.e.*, $\text{MSD}_{\text{exc}} = \langle z(t) - z(0) \rangle^2$) of the excitonic wavepacket depicted in Figure 3e of the main text (black line) and panel **b** (green line).

5 Animations

Animations of the excitonic wavepackets shown in Figure 3 of the main text (transport.mp4) and in Figure S5 (transport_delayed.mp4) are available for download in MPEG-4 format.

6 References

- (1) Forn-Díaz, P.; Lamata, L.; Rico, E.; Kono, J.; Solano, E. Ultrastrong coupling regimes of light-matter interaction. *Rev. Mod. Phys.* **2019**, *91*, 025005.
- (2) Jaynes, E. T.; Cummings, F. W. Comparison of quantum and semiclassical radiation theories with application to the beam maser. *Proc. IEEE* **1963**, *51*, 89–109.
- (3) Tavis, M.; Cummings, F. W. Approximate solutions for an N-molecule radiation-field Hamiltonian. *Phys. Rev.* **1969**, *188*, 692–695.
- (4) Michetti, P.; Rocca, G. C. L. Polariton states in disordered organic microcavities. *Phys. Rev. B.* **2005**, *71*, 115320.
- (5) Tichauer, R. H.; Feist, J.; Groenhof, G. Multi-scale Dynamics Simulations of Molecular Polaritons: the Effect of Multiple Cavity Modes on Polariton Relaxation. *J. Chem. Phys.* **2021**, *154*, 104112.
- (6) Warshel, A.; Levitt, M. Theoretical studies of enzymatic reactions: Dielectric, electrostatic and steric stabilization of carbonium ion in the reaction of lysozyme. *J. Mol. Biol.* **1976**, *103*, 227–249.
- (7) Boggio-Pasqua, M.; Burmeister, C. F.; Robb, M. A.; Groenhof, G. Photochemical reactions in biological systems: probing the effect of the environment by means of hybrid quantum chemistry/molecular mechanics simulations. *Phys. Chem. Chem. Phys.* **2012**, *14*, 7912–7928.
- (8) Ehrenfest, P. Bemerkung über die angenäherte Gültigkeit der klassischen Mechanik innerhalb der Quantenmechanik. *Z. Phys.* **1927**, *45*, 445–457.
- (9) Felicetti, S.; Fregoni, J.; Schnappinger, T.; Reiter, S.; de Vivie-Riedle, R.; Feist, J. Photoprotecting Uracil by Coupling with Lossy Nanocavities. *J. Chem. Phys. Lett.* **2020**, *11*, 8810–8818.

- (10) Ulusoy, I. S.; Vendrell, O. Dynamics and spectroscopy of molecular ensembles in a lossy microcavity. *J. Chem. Phys.* **2020**, *153*, 044108.
- (11) Antoniou, P.; Suchanek, F.; Varner, J. F.; Foley IV, J. J. Role of Cavity Losses on Nonadiabatic Couplings and Dynamics in Polaritonic Chemistry. *J. Phys. Chem. Lett.* **2020**, *11*, 9063–9069.
- (12) Hu, D.; Mandal, A.; Weight, B. M.; Huo, P. Quasi-diabatic propagation scheme for simulating polariton chemistry. *J. Chem. Phys.* **2022**, *157*, 194109.
- (13) Horta, B. A. C.; Merz, P. T.; Fuchs, P. F. J.; Dolenc, J.; Riniker, S.; Hünenberger, P. H. A GROMOS-Compatible Force Field for Small Organic Molecules in the Condensed Phase: The 2016H66 Parameter Set. *J. Chem. Theory. Comput.* **2016**, *12*, 3825–3850.
- (14) Hess, B.; Bekker, H.; Berendsen, H. J. C.; Fraaije, J. G. E. M. LINCS: A linear constraint solver for molecular simulations. *J. Comput. Chem.* **1997**, *18*, 1463–1472.
- (15) Berendsen, H.; Postma, J.; van Gunsteren, W.; la, A. D.; Haak, J. Molecular dynamics with coupling to an external bath. *J. Chem. Phys.* **1984**, *81*, 3684–3690.
- (16) Becke, A. D. A new mixing of Hartree-Fock and local density-functional theories. *J. Chem. Phys.* **1993**, *98*, 1372.
- (17) Lee, C. T.; Yang, W. T.; Parr, R. G. Development of the Colle-Salvet correlation-energy formula into a functional of the electron density. *Phys. Rev. B* **1988**, *37*, 785–789.
- (18) Yanai, T.; Tew, D. P.; Handy, N. C. A new hybrid exchange-correlation functional using the Coulomb-attenuating method (CAM-B3LYP). *Chem. Phys. Lett.* **2004**, *393*, 51–57.
- (19) Dunning, T. H. Basis Functions for Use in Molecular Calculations. I. Contractions of (9s5p) Atomic Basis Sets for the First-Row Atoms. *J. Chem. Phys.* **1970**, *53*, 2823–2833.
- (20) Runge, E.; Gross, E. K. U. Density-Functional Theory for Time-Dependent Systems. *Phys. Rev. Lett* **1984**, *52*, 997–1000.

- (21) Hirata, S.; Head-Gordon, M. Time-dependent density functional theory within the Tamm–Dancoff approximation. *Chem. Phys. Lett.* **1999**, *314*, 291–299.
- (22) Hess, B.; Kutzner, C.; van der Spoel, D.; Lindahl, E. GROMACS 4: Algorithms for Highly Efficient, Load-Balanced, and Scalable Molecular Simulation. *J. Chem. Theory Comput.* **2008**, *4*, 435–447.
- (23) Ufimtsev, I. S.; Martínez, T. J. Quantum Chemistry on Graphical Processing Units. 3. Analytical Energy Gradients and First Principles Molecular Dynamics. *J. Chem. Theory Comput.* **2009**, *5*, 2619–2628.
- (24) Titov, A. V.; Ufimtsev, I. S.; Luehr, N.; Martínez, T. J. Generating Efficient Quantum Chemistry Codes for Novel Architectures. *J. Chem. Theory Comput.* **2013**, *9*, 213–221.
- (25) Jorgensen, W. L.; Chandrasekhar, J.; Madura, J. D.; Impey, R. W.; Klein, M. L. Comparison of simple potential functions for simulating liquid water. *J. Chem. Phys.* **1983**, *79*, 926–935.
- (26) Duan, Y.; Wu, C.; Chowdhury, S.; Lee, M. C.; Xiong, G. M.; Zhang, W.; Yang, R.; Cieplak, P.; Luo, R.; Lee, T.; Caldwell, J.; Wang, J. M.; Kollman, P. A point-charge force field for molecular mechanics simulations of proteins based on condensed-phase quantum mechanical calculations. *J. Comput. Chem.* **2003**, *24*, 1999–2012.
- (27) Bayly, C. I.; Cieplak, P.; Cornell, W. D.; Kollman, P. A. A well-behaved electrostatic potential based method using charge restraints for deriving atomic charges - the RESP model. *J. Phys. Chem.* **1993**, *97*, 10269–10280.
- (28) Tomasi, J.; Mennucci, B.; Cammi, R. Quantum Mechanical Continuum Solvation Models. *Chem. Rev.* **2005**, *105*, 2999–3094.
- (29) Essmann, U.; Perera, L.; Berkowitz, M. L.; Darden, T.; Lee, H.; Pedersen, L. G. A smooth particle mesh Ewald potential. *J. Chem. Phys.* **1995**, *103*, 8577–8592.

- (30) Bussi, G.; Donadio, D.; Parrinello, M. Canonical sampling through velocity rescaling. *J. Chem. Phys.* **2007**, *126*, 014101.
- (31) Miyamoto, S.; Kollman, P. A. SETTLE: An analytical version of the SHAKE and RATTLE algorithms for rigid water molecules. *J. Comp. Chem.* **1992**, *18*, 1463–1472.
- (32) Becke, A. D. Density-functional thermochemistry. V. Systematic optimization of exchange-correlation functionals. *J. Chem. Phys.* **1997**, *107*, 8554–8560.
- (33) Schwartz, T.; Hutchison, J. A.; Leonard, J.; Genet, C.; Haacke, S.; Ebbesen, T. W. Polariton Dynamics under Strong Light-Molecule Coupling. *ChemPhysChem* **2013**, *14*, 125–131.
- (34) George, J.; Wang, S.; Chervy, T.; Canaguier-Durand, A.; Schaeffer, G.; Lehn, J.-M.; Hutchison, J. A.; Genet, C.; Ebbesen, T. W. Ultra-strong coupling of molecular materials: spectroscopy and dynamics. *Faraday Discuss.* **2015**, *178*, 281–294.
- (35) Rozenman, G. G.; Akulov, K.; Golombek, A.; Schwartz, T. Long-Range Transport of Organic Exciton-Polaritons Revealed by Ultrafast Microscopy. *ACS Photonics* **2018**, *5*, 105–110.
- (36) Granucci, G.; Persico, M.; Toniolo, A. Direct semiclassical simulation of photochemical processes with semiempirical wave functions. *J. Chem. Phys.* **2001**, *114*, 10608–10615.
- (37) Frisch, M. J.; Trucks, G. W.; Schlegel, H. B.; Scuseria, G. E.; Robb, M. A.; Cheeseman, J. R.; Scalmani, G.; Barone, V.; Petersson, G. A.; Nakatsuji, H.; Li, X.; Caricato, M.; Marenich, A. V.; Bloino, J.; Janesko, B. G.; Gomperts, R.; Mennucci, B.; Hratchian, H. P.; Ortiz, J. V.; Izmaylov, A. F.; Sonnenberg, J. L.; Williams-Young, D.; Ding, F.; Lipparini, F.; Egidi, F.; Goings, J.; Peng, B.; Petrone, A.; Henderson, T.; Ranasinghe, D.; Zakrzewski, V. G.; Gao, J.; Rega, N.; Zheng, G.; Liang, W.; Hada, M.; Ehara, M.; Toyota, K.; Fukuda, R.; Hasegawa, J.; Ishida, M.; Nakajima, T.; Honda, Y.; Kitao, O.; Nakai, H.; Vreven, T.; Throssell, K.; Montgomery, J. A., Jr.; Peralta, J. E.; Ogliaro, F.; Bearpark, M. J.; Heyd, J. J.; Brothers, E. N.; Kudin, K. N.; Staroverov, V. N.; Keith, T. A.; Kobayashi, R.; Normand, J.; Raghavachari, K.;

- Rendell, A. P.; Burant, J. C.; Iyengar, S. S.; Tomasi, J.; Cossi, M.; Millam, J. M.; Klene, M.; Adamo, C.; Cammi, R.; Ochterski, J. W.; Martin, R. L.; Morokuma, K.; Farkas, O.; Foresman, J. B.; Fox, D. J. Gaussian~16 Revision C.01. 2016; Gaussian Inc. Wallingford CT.
- (38) Modi, V.; Donnini, S.; Groenhof, G.; Morozov, D. Protonation of the Biliverdin IX α Chromophore in the Red and Far- Red Photoactive States of a Bacteriophytochrome. *J. Phys. Chem. B* **2019**, *123*, 2325–2334.
- (39) Agranovich, V. M.; Gartstein, Y. N. Nature and Dynamics of Low-Energy Exciton Polaritons in Semiconductor Microcavities. *Phys. Rev. B* **2007**, *75*, 075302.
- (40) Lidzey, D. G.; Bradley, D. C.; Armitage, A.; Walker, S.; Skolnick, M. S. Photon-Mediated Hybridization of Frenkel Excitons in Organic Semiconductor Microcavities. *Science* **2000**, *288*, 1620–1623.
- (41) Dutta, A.; Tiainen, V.; Duarte, L.; Markesevic, N.; Morozov, D.; Qureshi, H. A.; Groenhof, G.; Toppari, J. J. Ultra-fast photochemistry in the strong light-matter coupling regime. *Chemrxiv* **2023**,
- (42) Staroverov, V. N.; Scuseria, G. E.; Tao, J.; Perdew, J. P. Comparative assessment of a new nonempirical density functional: Molecules and hydrogen-bonded complexes. *J. Chem. Phys.* **2003**, *119*, 12129–12137.
- (43) Picconi, D. Nonadiabatic quantum dynamics of the coherent excited state intramolecular proton transfer of 10-hydroxybenzo [h] quinoline. *Photochem. Photobiol. Sci.* **2021**, *20*, 1455–1473.